Journal of Power Sources 290 (2015) 14–24

Contents lists available at ScienceDirect

Journal of Power Sources

journal homepage: www.elsevier.com/locate/jpowsour

A comprehensive equivalent circuit model of all-vanadium redox flow battery for power system analysis

Yu Zhang [a], Jiyun Zhao [b, *], Peng Wang [a], Maria Skyllas-Kazacos [c], Binyu Xiong [a], Rajagopalan Badrinarayanan [a]

[a] EXQUISITUS, Centre for E-City, School of Electrical & Electronic Engineering, Nanyang Technological University, Singapore 639798, Singapore
[b] Department of Mechanical and Biomedical Engineering, City University of Hong Kong, Kowloon, Hong Kong
[c] School of Chemical Engineering, The University of New South Wales, UNSW Sydney, NSW 2052, Australia

HIGHLIGHTS

- A comprehensive electrical VRB model is proposed for power grid analysis.
- Inherent features of shunt current, ion diffusion and pump power are included.
- Least square method is used to identify dynamic and stationary characteristics.
- The simulation results match with experimental data.
- Sensitivity analyses have been done to study the inherent features.

ARTICLE INFO

Article history:
Received 5 February 2015
Received in revised form
31 March 2015
Accepted 29 April 2015
Available online 15 May 2015

Keywords:
Vanadium redox flow battery
Electrical equivalent circuit model
Hydraulic modeling
Shunt current

ABSTRACT

Electrical equivalent circuit models demonstrate excellent adaptability and simplicity in predicting the electrical dynamic response of the all-vanadium redox flow battery (VRB) system. However, only a few publications that focus on this topic are available. The paper presents a comprehensive equivalent circuit model of VRB for system level analysis. The least square method is used to identify both steady-state and dynamic characteristics of VRB. The inherent features of the flow battery such as shunt current, ion diffusion and pumping energy consumption are also considered. The proposed model consists of an open-circuit voltage source, two parasitic shunt bypass circuits, a 1st order resistor-capacitor network and a hydraulic circuit model. Validated with experimental data, the proposed model demonstrates excellent accuracy. The mean-error of terminal voltage and pump consumption are 0.09 V and 0.49 W respectively. Based on the proposed model, self-discharge and system efficiency are studied. An optimal flow rate which maximizes the system efficiency is identified. Finally, the dynamic responses of the proposed VRB model under step current profiles are presented. Variables such as SOC and stack terminal voltage can be provided.

1. Introduction

With the increasing development of renewable energy such as solar and wind, large scale energy storage systems have become especially critical for the stability of micro-grids due to the stochastic behavior and intermittency of the renewable sources [1,2]. Among the existing energy storage technologies, the all-vanadium redox flow battery (VRB) initialized by Skyllas-Kazacos and co-workers [3,4] has been widely investigated and commercialized due to its outstanding advantages such as capacity and output power design independency, cross contamination elimination, infinite life cycle and high energy efficiency [5–7].

There are different scalabilities for battery modeling. The electrochemical models of the VRB [8–10] are based on the conservation law of mass, species concentration and energy. These models give insights on membrane investigation, electrodes design, electrolyte selection and flow frame optimization. Since the electrochemical model is complex and time consuming however, it is necessary to develop a practical model for control purposes in power grid analysis [11,12].

* Corresponding author.
E-mail address: jiyuzhao@cityu.edu.hk (J. Zhao).

http://dx.doi.org/10.1016/j.jpowsour.2015.04.169
0378-7753/

Nomenclature

L	length (cm)
D	thickness/diameter (cm)
W	width (cm)
E	potential (V)
T	temperature (K)
R	gas constant (8.314 J mol^{-1} K^{-1}))
F	Faraday constant (96487C mol^{-1})
p	pressure (Pa or psi)
A	cross area (cm^2)
i	current density (mA cm^{-2})
ρ	density (Kg m^{-3})
c	concentration (M)
P	power (W)
h	friction loss/minor loss
$\tilde{R}$	hydraulic resistance (Pa s m^{-3})
η	efficiency/diffusion ratio
n	cell number
H	height (cm)
μ	viscosity (Kg m^{-1} s^{-1})
σ	conductivity (Ω^{-1} cm^{-1})
V	volume (L)
SOC	state of charge
Q	flow rate ($Lmin^{-1}$)
s	Laplace operator
a	fix coefficient
Re	Reynolds number

Subscript

out	outlet
In	inlet
Man/M	Manifold
int	internal
A	anode
C	cathode
G	Guide channel
diff	diffusion
opv	open circuit voltage
cha/dis	charge/discharge
sys	system
en	energy

Electric equivalent circuit models demonstrate excellent adaptability and simplicity in predicting the electrical dynamic response of the VRB system and are proper candidates for system level control. Many researchers propose different topologies and identification methods for electric circuit models. Chahwan [13] proposed an equivalent circuit model with a voltage source represent the stack voltage, a controlled current source and a fixed loss resistance representing parasitic losses of pumps, reaction resistance and electrode capacitors. The drawback is that the parameter identification process is based on estimated values of the battery and model validation is not provided. Robert Fares [14] describes a battery model as a voltage source in series with an internal resistance, but the identification method is also not clearly stated.

The electric model parameters are extracted based on the experimental charging and discharging curves. One of the identification methods is to analyze the electrode overpotentials by electrochemical impedance spectroscopy (EIS) [15]. The capacitance and resistance are estimated by measurements under a wide range of frequencies. But EIS is only applicable to a single cell measurement, so an easy and feasible method needs to be proposed for a large battery stack. Another identification method is to apply an extended Kalman filter to set up the model [16]. The extended Kalman filter method can effectively reduce the measurement noise and the simulation results match with the practical data. But the identification of the dynamic parameters largely depends on the selection of its initial value. Furthermore, some other factors such as the shunt current and the pump consumption are not considered in the previous model.

The shunt current is caused by the potential gradient across the stacks that drives the ions through the common manifolds [17,18]. The pump power is a parasitic loss that needs to count in the model as well. In previous studies, Xiong et al. [19] proposed a hydraulic method to estimate the pump power losses, while Tang et al. [20] included both pumping and shunt current losses in the overall battery efficiency calculation for both variable and constant flow-rate operation.

In this paper, a comprehensive equivalent circuit model of VRB with the effects of shunt current and pump power is proposed. In the first part, the shunt current model is set up by the series and parallel connected cell resistance and electrolyte resistance. The hydraulic model predicts the pump power loss based on hydraulic design of stack and tank by the empirical equations. Then, the charging and discharging curves are applied to identify the RC network in the model by using the least square method. After model establishment, the self-discharge caused by ion diffusion across the membrane, the parasitic losses associated with shunt currents, as well as the battery performance under different terminal currents and electrolyte flow rates are analyzed. Lastly, the simulated dynamic responses to step currents are shown.

2. Structure of VRB system

A typical VRB system includes at least one stack, two electrolyte tanks, two circulating pumps and other components. The VRB structure is divided into two parts, namely, the external hydraulic circuit and the VRB stack [21]. The proposed model in this paper is based on a practical 1 kW/1 kWh VRB system established by Kim et al. [22].

2.1. External hydraulic circle

Since the VRB system is symmetrical, one half-side of the whole system is shown in Fig. 1(a). The mixed acid (2 M $VOSO_4 \cdot xH_2O$ + 2 M H_2SO_4 + 5 M HCl) was used as electrolyte, which can avoid electrolyte precipitation of temperature above 40 °C. Each of anolyte and catholyte with volume of 30 L were contained in two electrolyte tanks. Through 1″ PVC pipe, electrolyte flows from tank outlet to pump inlet. 1/2″ PVC pipe was used in other places. The diameters and lengths of each pipe, bends, sudden contraction and expansion are all marked in the figure. All of these geometric parameters are required for the hydraulic circuit model.

2.2. VRB stack structure

Normally, the geometry of VRB stack is complex and is composed of multiple cells, each comprising bipolar or end plate −graphite felt − membrane − graphite felt −bipolar or end plate, which are piled to form a stack. The 1 kW VRB stack proposed by Kim consists of 15 unit cells. Between each cell, 1" (1.27 cm)

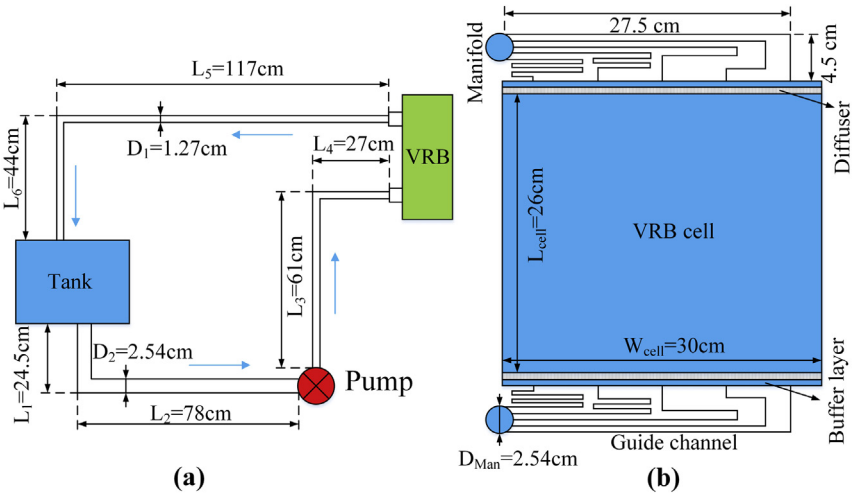

Fig. 1. Hydraulic structure of VRB system proposed by Kim [22], (a). External hydraulic half-circuit of VRB system; (b). VRB cell structure.

manifolds are used to connect the electrolyte channel together. Fig. 1(b) illustrates the flow frame plate of the 1 kW VRB stack that includes five electrolyte guide channels (32 cm effective length with 1 mm width and 3 mm depth). Each flow frame plate is connected to a common buffer layer and diffusers prior to the porous electrodes (26 cm length, 30 cm wide and 3 mm depth). Based on these geometric parameters, shunt current and the pressure drop within the VRB stack can be estimated.

In addition to the geometric parameters illustrated in Fig. 1(a) and (b), other parameters such as electrolyte density, viscosity or conductivity can be found in Refs. [22], which are summarized in Table 1.

3. Comprehensive equivalent circuit model for VRB

An equivalent electrical model consists of a SOC dependent voltage source in series with resistor-capacitor (RC) networks, resembling the model used for Li-ion and NiMH batteries [16]. However, the inherent features of VRB, shunt current, vanadium ion diffusion across the membrane, as well as the pump consumption cannot be ignored. The comprehensive model proposed in this paper takes into account of all these features, as shown in Fig. 2. The model consists of an open circuit potential, E_{opv}, two controlled current sources, I_{diff} and I_{shunt}, that correspond to the effect of membrane diffusion, shunt current, RC network circuit that stands for the stationary and the dynamic characteristics of electrical response, and a hydraulic circle model that is used to predict the power consumption of pumps. In the following sections, all these four units will be explained in detail.

Table 1
Parameters of the VRB system [22].

Number of cells, n_{cell}	15
Dimension of half-cell	30 × 26 × 0.3 (cm)
Permeability of porous electrode, k	1.685×10^{-10} m^2
Diameter of Manifold, D_{Man}	2.54 cm
Height of Manifold for each cell, H_{Man}	1.65 cm
Dimension of guide channel (effective value)	32 × 0.1 × 0.3 (cm)
Electrolyte density, ρ	1400 kg m^{-3}
Electrolyte viscosity, μ	0.006 kg m^{-1} s^{-1}
Electrolyte conductivity, σ	0.2 Ω^{-1} cm^{-1}
Internal cell resistance, r_{int}	1.0 Ω cm^2
Tank volume, V_{tank}	30 L
Concentration of V ion, c_v	2 M
Operating temperature of VRB,T	42.5 °C
Diffusion ratio of the membrane, η_{diff}	0.95

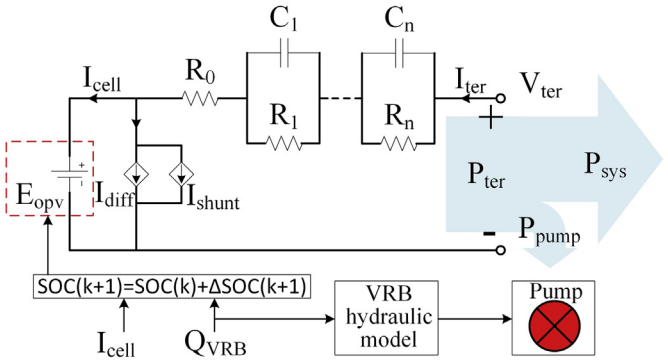

Fig. 2. Proposed comprehensive electrical model for VRB.

3.1. Nernst equation and state-of-charge

The open circuit voltage represents the battery electromotive force at the ideal state, which depends on the vanadium species concentration and on the operation temperature. This potential can be obtained by the Nernst equation [23],

$$E_{ocv} = E^{\theta} + \frac{RT}{zF}\ln\left[\left(\frac{(c_{V^{2+}})\left(c_{VO_2^+}\right)\left(c_{H^+}^2\right)}{(c_{VO^{2+}})(c_{V^{3+}})}\right)\left(\frac{(\gamma_{V^{2+}})\left(\gamma_{VO_2^+}\right)\left(\gamma_{H^+}^2\right)}{(\gamma_{VO^{2+}})(\gamma_{V^{3+}})}\right)\right] \quad (1)$$

where E^{θ} is the standard electrode potential, c_i denotes the concentrations of species I and γ is the activity coefficients.

The concentration of protons in the catholyte is difficult to estimate due to ion pairing equilibria in the solution and it is usually considered as 1 M. Alternatively, it is assumed to remain constant and is incorporated into the formal electrode potential that is experimentally measured at 50% State of charge (SOC) [24]. The second term of activity coefficient product in brackets is approximated to be 1 unit reflecting the cancellation of each species, but can also be incorporated into the experimentally determined standard electrode potential [23].

The Nernst equation is simplified as,

$$E_{ocv} = E_0 + \frac{2RT}{F}\ln\left(\frac{SOC_{cell}}{1 - SOC_{cell}}\right) \quad (2)$$

By fitting the experimental data [25], the value of E_0 was set to 1.39 V according to previous articles [23,24]. The SOC of battery is an indication of energy level of the battery, which is related to the concentrations of the different vanadium species. SOC value varies from 0 to 1, where '0' stands for fully discharged; '1' stands for fully charged.

$$SOC = \frac{c_{V^{2+}}}{(c_{V^{2+}}) + (c_{V^{3+}})} = \frac{c_{VO_2^+}}{\left(c_{VO_2^+}\right) + (c_{VO^{2+}})} \tag{3}$$

The electrolyte SOC reflects the overall vanadium ion concentration level of the battery and indeed the value is proportional to the quantity of electrons that have been transferred into the stack. Therefore, SOC_{tank} is related to the initial SOC of electrolyte in the tank, the size of the tank, V_{tank}, and the current, I_{cell}, that flows through the cell stack.

$$SOC_{tank}(t) = SOC_{tank}(0) + \frac{n_{cell}}{FV_{tank}c_v}\int_0^t I_{cell}d\tau \tag{4}$$

The cell SOC is needed to solve the Nernst potential as shown in Eq. (2). Since the SOC inside the cell is not uniformly distributed, the mean value of $SOC_{cell,in}$ and $SOC_{cell,out}$ is used to replace the distributed value [21].

$$SOC_{cell} = \frac{SOC_{cell,in} + SOC_{cell,out}}{2} \tag{5}$$

For simplicity, SOC_{cell} is related to the cell current I_{cell}, the electrolyte flow rate Q_{vrb}, the inlet SOC and the cell number n_{cell}. The average SOC of cell can be obtained as,

$$SOC_{cell}(t) = SOC_{tank}(t) + \frac{n_{cell}I_{cell}}{2FQ_{vrb}c_v} \tag{6}$$

3.2. Shunt current and the effects of vanadium ion diffusion

Shunt currents are caused by the potential gradient across the cell stack that drives the ions moving through the conducting manifold and guide channels. For higher coulombic efficiency, minimization of shunt current is important and this is achieved by increasing the electrolyte path resistance with long narrow electrolyte guide channels and common manifolds [26].

A typical electrical circuit of shunt current in a flow battery is shown in Fig. 3(a) [27], where the current source I_{ter} is the terminal current and R_{cell} is the cell resistance. The subscripts 'M', 'G', 'A', 'C' represent the manifold, guide channel, anode and cathode respectively, while the superscripts of 'in' and 'out' stand for inlet and outlet of the flow battery [17].

The ionic resistance of the channel and manifold are calculated on the basis of specific flow-frame design and electrolyte conductivity determined according to Eq. (7),

$$R = \frac{l}{\sigma A} \tag{7}$$

where l is the effect length, A is the cross sectional area and σ is the electrolyte conductivity. All these values are listed in Fig. 1(b) and Table 1.

The shunt loss predicted for 1 kW VRB stack is shown in Fig. 3(b). During the charge process, the shunt current reduces the actual cell current available for electrochemical reactions, while during discharge process, the actual cell current is increased due to the shunt current. The coulombic efficiency will be reduced due to the shunt current losses. In this work, the effect of the shunt current is not obvious (less than 0.15 A). However, it will increase with increasing series number of cells, which makes the effect of shunt current an important factor in large-scale VRB system.

The shunt current model in Fig. 3(a) is lumped as a controlled current source in the overall VRB model in Fig. 2. The total shunt current of VRB stack is the average value of all single cells, as shown in Fig. 3(b). If the terminal current 'I_{ter}' and the open circuit voltage of single cell 'E_{cell}' are known, the total shunt current of VRB stack 'I_{shunt}' can be obtained.

In addition to the shunt current, the diffusion of vanadium ions also has a significant impact on the coulombic efficiency [28]. When there is a vanadium ion concentration difference across the membrane, self-discharge and side reactions will occur and reduce the capacity of battery in long-term cycling [29,30]. Based on the conservation of mass, Tang's paper [31] provides a dynamic model to predict the capacity loss caused by the diffusion effect and battery side reactions. However, Tang's model is complex and time-consuming for power grid analysis. A simplified equation is used to estimate the effect of diffusion effect [32],

$$I_{diff} = \left(\frac{\eta_{diff}}{2 - \eta_{diff}}\right)|I_{ter}| \tag{8}$$

where η_{diff}, is the complementary part of coulomb efficiency, η_{CE}, representing the self-discharge loss due to the ion diffusion in each cycle of charge/discharge. The diffusion ratio is defined as $\eta_{diff} = 1 - \eta_{CE}$. According to the literature of [22], i.e. Kim's report, the coulomb efficiency equals to 95%, thus the diffusion ratio η_{diff} is set as 5%. The item 'I_{diff}' is used to estimate the self-discharge current by ion diffusion.

It should be mentioned however, that this assumption does not account for the differential transfer of the different vanadium ions across the membrane that leads to a build-up in one half-cell and a depletion in the other. While the Eq. (8) used here accounts for coulombic efficiency losses therefore, it cannot estimate the capacity loss from the differential vanadium ion transfer across the membrane. Nor does it account for capacity loss associated with side reactions such as hydrogen evolution during charging and air oxidation of V^{2+} in the negative half-cell. For simplicity however, these effects have been ignored in the present model.

3.3. RC network identification

Compared with the electrochemical model, an equivalent circuit model is suited for describing the electrical behavior of the VRB, which makes it adaptable in electrical and control analysis owing to its simplicity. Usually, the model consists of an open-circuit potential, an internal resistance, and 'n' order RC pairs [16].

The experimental VI curves from Kim's article [22] have been divided into two parts, namely, the dynamic zone and the stationary zone, which is shown by using circles in Fig. 5(a). Based on the beginning part of Kim's experimental data, a 1st order RC pair is adopted to identify the dynamic characteristic of VRB stack. After several seconds, the capacitor of the 1st order RC pair has been fully charged. The VRB's terminal voltage reaches into steady-state. In order to identify the stationary characteristic of VRB stack, a resistor network is used in this work. Based on the latter half of Kim's experimental data, the unknown parameters of the resistor network can be obtained. Finally, the 1st order RC pair of dynamic model and the resistor of stationary model are considered together to form a final electrical circuit model. Therefore, the proposed model can reflect both of the dynamic and stationary characteristics of VRB stack.

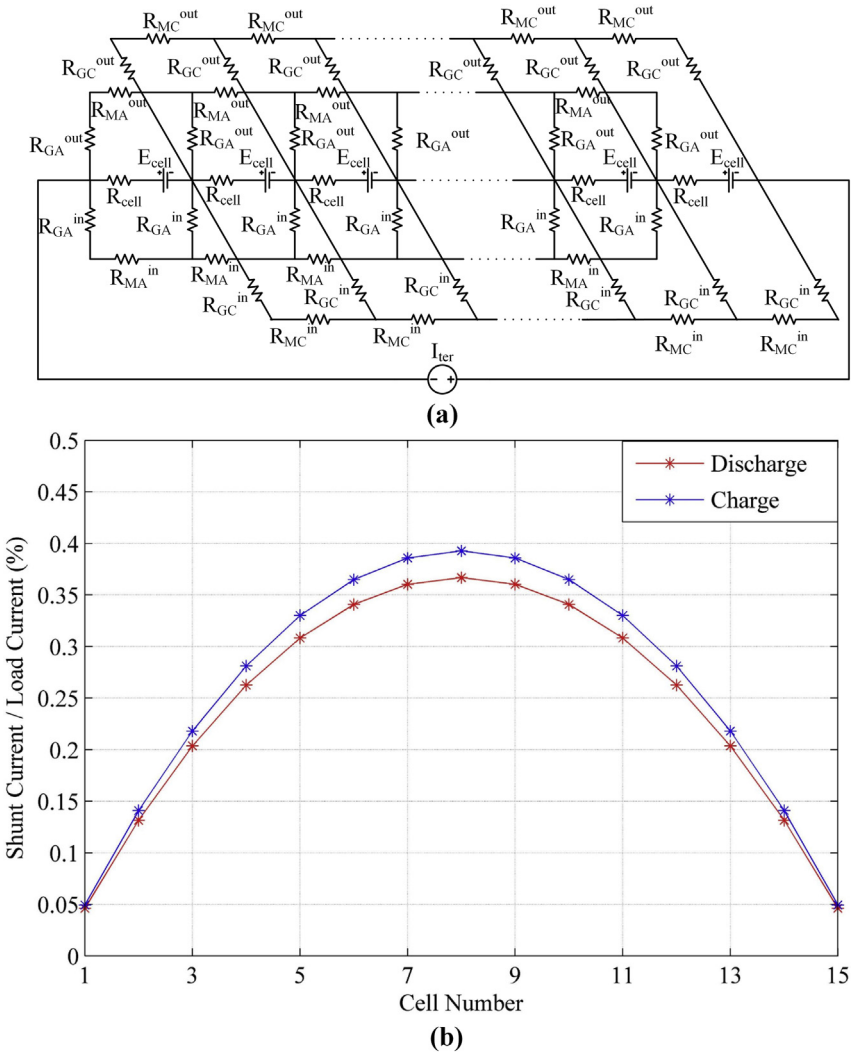

Fig. 3. Shunt current model and simulation result, (a). Electrical circuit analogy of a bipolar stack [27]; (b). Prediction of shunt current distribution in the 15 cells stack at 50 mA cm^{-2} and 50% SOC.

As shown in Fig. 4(a), a 1st order RC pair is adopted to identify the dynamic characteristic of VRB stack. In order to identify the dynamic characteristic of VRB system, the beginning part of Kim's experimental data has been used [22], as shown in Fig. 5(a). Moreover, it can be reasonable assumed that before the VRB stack has been charged/discharged, the terminal current equals to zero. And the initial open circuit voltage can be estimated by using Nernst equation (initial SOC are 0.15 and 0.85 for charge and discharge respectively [22]). If the step input current and its corresponding voltage response are known, all components shown in Fig. 4(a) can be identified by using least square method. Based on KVL theory it, has:

$$\begin{cases} \dfrac{E_{opv}}{s} - V_{ter} - I_1R_0 - (I_1+I_2)R_1 = 0 \\ \dfrac{U_{c1}\left(0^-\right)}{s} - \dfrac{I_2}{C_1 s} - (I_1+I_2)R_1 = 0 \end{cases} \tag{9}$$

where I_1 equals to I_{ter}, after rearranging, the transfer function between the terminal voltage and the terminal current can be obtained as,

$$V_{ter} = \frac{E_{opv}}{s} - \frac{U_{c1}(0^-)C_1R_1}{1+C_1R_1 s} + I_1\left(-R_0 - R_1 + \frac{R_1^2C_1 s}{1+C_1R_1 s}\right) \tag{10}$$

$$tf(s) = \frac{\partial \Delta V_{ter}}{\partial I_{ter}} = \frac{b_1 s + b_2}{a_1 s + 1} \tag{11}$$

where

$$\begin{cases} a_1 = C_1R_1 \\ b_1 = -R_0C_1R_1 \\ b_2 = -R_0 - R_1 \end{cases} \tag{12}$$

Eq. (11) can be further rewritten in time domain,

$$a_1\Delta V_{ter}'(t) + \Delta V_{ter}(t) = b_1 I_{load}'(t) + b_2 I_{load}(t) \tag{13}$$

or,

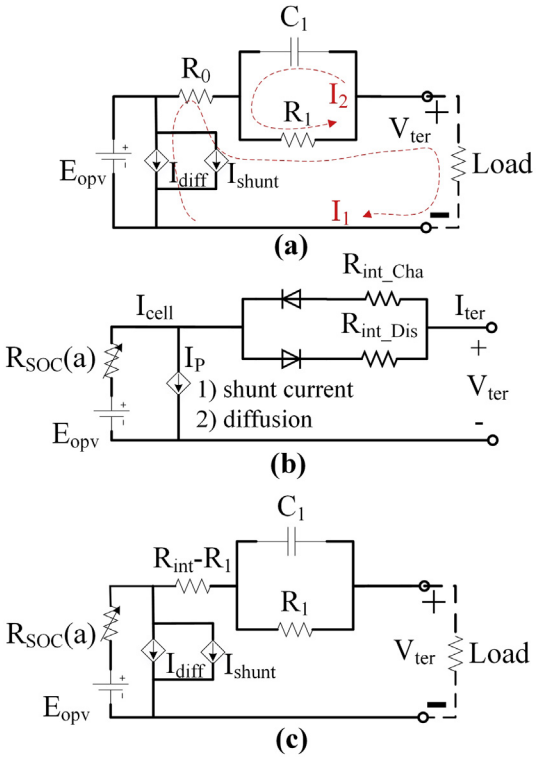

Fig. 4. Electrical circuit model of VRB, (a). Electrical circuit model of VRB (dynamic zone); (b). Electrical circuit model of VRB (stationary zone); (c). Final electrical circuit model of VRB.

$$\Delta V_{ter}(t) = -\frac{1}{a_1}\int_0^t \Delta V_{ter}(\tau)d\tau + \frac{b_1}{a_1} I_{load}(t) + \frac{b_2}{a_1}\int_0^t I_{load}(\tau)d\tau \tag{14}$$

To calculate the integration from a set of sample data, the numerical integrator can be used to transform the integration into discrete data, Combined with experimental data, Eq. (14) can be rewritten into a simple form,

$$\gamma(t) = \phi(t)\theta + e \tag{15}$$

where 'e' is measurement noise and 'θ' is the matrix of unknown parameter,

$$\begin{cases} \gamma(t) = \Delta V_{ter}(t) \\ \theta = \left[\dfrac{1}{a_1} \quad \dfrac{b_1}{a_1} \quad \dfrac{b_2}{a_1}\right]^T \\ \phi(t) = \left[-\displaystyle\int_0^t \Delta V_{ter}(\tau)d\tau \quad I_{load}(t) \quad \int_0^t I_{load}(\tau)d\tau\right] \end{cases} \tag{16}$$

Since there are many measure points distributed in different time, all of the data are combined to get,

$$\Gamma = \Psi\theta + \Delta \tag{17}$$

where Δ is measurement noise array and $\Psi = \begin{bmatrix} \phi(t_1) \\ \phi(t_2) \\ \vdots \\ \phi(t_N) \end{bmatrix}$,

$\Gamma = \begin{bmatrix} \gamma(t_1) \\ \gamma(t_2) \\ \vdots \\ \gamma(t_N) \end{bmatrix}$

As the rows in Ψ are independent to each other, $\Psi^T\Psi$ is non-singular. Thus the ordinary least squares method can be used to find out the unknown parameters

$$\hat{\theta} = \left(\Psi^T\Psi\right)^{-1}\Psi^T\Gamma \tag{18}$$

The unknown parameters can be identified from

$$\begin{bmatrix} a_1 \\ b_1 \\ b_2 \end{bmatrix} = \begin{bmatrix} 1/\theta(1) \\ \theta(2)/\theta(1) \\ \theta(3)/\theta(1) \end{bmatrix} \tag{19}$$

and the value of R_0 R_1 and C_1 can be obtained as,

$$\begin{cases} R_0 = -b_1/a_1 \\ R_1 = \dfrac{b_1}{a_1} - b_2 \\ C_1 = \dfrac{a_1^2}{b_1 - a_1 b_2} \end{cases} \tag{20}$$

Besides the 1st order RC pair model for VRB's dynamic performance, a steady-state resistor circuit is shown in Fig. 4(b), which is used for identifying VRB's stationary performance. The stationary model includes an internal resistor network, R_{int_cha} and R_{int_Dis} for charging and discharging respectively.

To reduce the complexity of including a thermal model, the operating temperature of VRB stack is set to a constant value of 42.5 °C based on experimental data [22]. Meanwhile, according to Baccino's analysis [33], the 'derived' SOC by theoretical calculation may differ from the 'true' SOC inside the stack; and the internal resistance of VRB is a function of cell SOC. In order to correct the inaccuracy of SOC, a fitting coefficient 'a' is added in front of the natural logarithm term of the original Nernst equation, as described in Eq. (21),

$$V_{ter} = n_{cell} \times \left(E_0 + a\frac{2RT}{F}\ln\left(\frac{Soc_{cell}}{1 - Soc_{cell}}\right)\right) + I_{ter}R_{int} \tag{21}$$

Similar with the dynamic zone identification, the value of 'a' and 'R_{int}' can be easily obtained by using the least square method.

Finally, based on both identifications of dynamic zone and stationary zone, 5 unknown parameters can be figured out. They are 'R_0', 'R_1', 'C_1', 'R_{int}' and 'a'. However, these 5 parameters belong to two different models. The VRB's dynamic characteristic is primarily determined by the R_1C_1 pair of dynamic model and its stationary characteristic is mainly determined by 'R_{int}' and 'a' of the stationary model. Therefore, in order to build an accurate model in both dynamic and stationary zone. The 'R_1C_1' pair as well as 'R_{int}' and 'a' are selected to represent the electrical characteristics of the VRB system. The final electrical circuit model of the VRB system is shown in Fig. 4(c).

3.4. Hydraulic model and pump power consumption

Mechanical power drives the electrolyte flowing through the hydraulic circuit of the VRB. In order to determine the power consumption of the pumps, it is necessary to model the hydraulic circuits first and the pump consumption can be estimated under any operating conditions.

As introduced in the previous section, the hydraulic circuit consists of an external electrolyte circuit and a VRB stack. The stack is comprised of several cells aligned hydraulically in parallel as shown in Fig. 1(b). Most of the pressure drop occurs within the VRB stack of which about 70% is due to the pressure drop in the felt electrodes [22]. The felt electrode is similar to a porous sponge

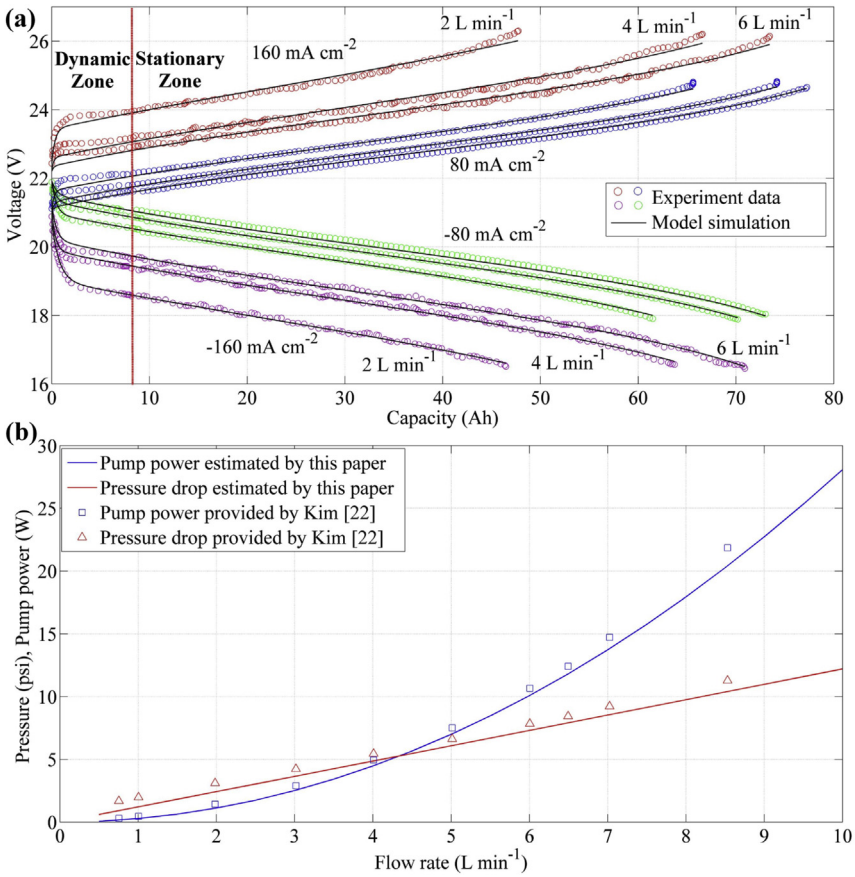

Fig. 5. Comparison between simulation results and experimental data [22]; (a). Stack voltage under various flow rates and various current densities; (b). Pump power and pressure drop within VRB.

structure and its hydraulic resistance can be estimated by using Darcy equation,

$$\tilde{R}_{cell} = \frac{\mu L_{cell}}{kW_{cell}D_{cell}} \tag{22}$$

where 'k' is the permeability of the porous electrode and 'μ' is the electrolyte viscosity. The total pressure drop of VRB stack can be obtained as,

$$\Delta p_{stack} = Q_{vrb}\frac{\tilde{R}_{cell}}{0.7n_{cell}} \tag{23}$$

From the external circuit as shown in Fig. 1(a), two kinds of losses namely form loss and friction loss need to be considered. Form loss happens when the electrolyte changes its direction and velocity and the roughness of pipe and the fluid viscosity lead to friction loss [19].

To calculate the pressure drop within the external circuit, the Reynolds number 'Re' needs to be calculated to determine whether the flow is laminar or turbulent.

$$\mathrm{Re} = \frac{\rho V_s D}{\mu} \tag{24}$$

where 'V_s' is the flow velocity of electrolyte and 'D' is the hydraulic diameter.

With the value of Reynolds number 'R_e', the friction factor 'f_i' is determined by Eq. (25) for a laminar flow and Eq. (26) for a turbulent flow.

$$f_i = \frac{64}{Re} \quad (Re < 2000) \tag{25}$$

$$f_i = 0.316Re^{-0.25} \quad (4000 < Re < 10000) \tag{26}$$

The friction loss '$h_{f,i}$' can be calculated with Darcy–Weisbach equation,

$$\mathrm{h_{f,i}} = f_i\frac{L_i}{D_i}\frac{V_{s,i}^2}{2g} \tag{27}$$

where 'L' is the length of the pipe and 'g' is the acceleration due to gravity.

The minor loss '$h_{m,i}$' is determined by Eq. (28), where the minor loss coefficients '$k_{L,i}$' is given in Table 2 [21].

$$\mathrm{h_{m,i}} = k_{L,i}\frac{V_{s,i}^2}{2g} \tag{28}$$

Finally, combined the effects of fraction loss and minor loss, the pressure drop of the external hydraulic circle can be determined by the Bernoulli equation,

$$\Delta p_{hydr} = \rho g\left(h_{\mathrm{work}} - \frac{\Delta V_{s,i}^2}{2g} - \Delta z - \mathrm{h_{f,i}} - \mathrm{h_{m,i}}\right) \tag{29}$$

where the first term 'h_{work}' stands for the work done to the system, the second term stands for the change of potential energy and the

Table 2
Coefficients of minor loss [21].

Components	Loss coefficients $k_{L,i}$
Flanged 90° elbow	0.2
From tank into pipe	0.4
From pipe into tank	1
From 1″ pipe into 0.5″ pipe	0.33
From 0.5″ pipe into 1″ pipe	0.5625

third term stands for the change of the kinetic energy. For computational simplicity, all these three terms are assumed to be zero.

The corresponding mechanical power 'P_{pump}'is calculated as,

$$P_{pump} = \left(\Delta p_{stack} + \Delta p_{hydr}\right) Q_{vrb} / \eta_{pump} \tag{30}$$

'η_{pump}' is the transfer efficiency of pump with a value is set to 0.5 [22].

4. Verification

In this section, the proposed VRB equivalent electrical circuit model is validated in two aspects, namely, electrical response and the pump power consumption. The corresponding experimental data are obtained from earlier work in the same area [22].

4.1. Terminal voltage validation

The experimental values of charge/discharge at different flow rates and different current densities are obtained from Ref. [22] as shown in Fig. 5(a). The three different flow rates of 2, 4 and 6 Lmin^{-1} and the four different current densities of −160, −80, 80, 160 mA cm^{-2} are tested. Based on these results and the least square method introduced in section 3.3, the parameter identification results are shown in Table 3.

In Fig. 5(a), the identification results are compared with the practical experimental data, where the simulation results are plotted as black lines and the experimental data are marked as circles. It is clear that the simulation results demonstrate a good degree of accuracy in both the dynamic region as well as the stationary region. The mean error of all these twelve curves equals 0.09 V confirming that the simulation results fit the practical data. However, due to the lack of other experimental data, when the operating conditions are changed, all unknown parameters can be obtained by interpolation. To ensure the correctness and reasonableness of the fitting results, more experimental measurements are required to obtain the accurate fitting results under different operational conditions using the methodology described in this paper.

Table 3
Identification of parameters under different flow rates and current densities.

i_{ter}(mA cm^{-2})	Q_{vrb}(L min^{-1})	a	R_{int} (Ω)	R_0 (Ω)	R_1 (Ω)	C_1 (F)
160	2	1.6999	0.0294	0.0209	0.0085	1.16E+03
160	4	1.4537	0.0248	0.0217	0.0031	1.90E+03
160	6	1.3364	0.0231	0.0218	0.0013	4.48E+03
80	2	1.3203	0.0320	0.0222	0.0098	1.34E+03
80	4	1.2534	0.0291	0.0247	0.0044	3.77E+03
80	6	1.2176	0.0271	0.0252	0.0019	6.57E+03
−80	2	1.3461	0.0222	0.007	0.0152	1.77E+03
−80	4	1.2738	0.0191	0.0102	0.0089	2.84E+03
−80	6	1.2471	0.0168	0.0103	0.0065	4.42E+03
−160	2	1.5531	0.0244	0.0107	0.0137	1.61E+03
−160	4	1.3921	0.0201	0.0104	0.0097	1.11E+03
−160	6	1.3491	0.0186	0.0102	0.0084	1.65E+03

4.2. Pump power consumption validation

Fig. 5(b) shows the pump power consumption and the pressure drop within the VRB system. The hydraulic model introduced in this paper shows good agreement with the results provided by Kim [22]. It is clear that the pressure drop increases linearly with the flow rate with an overall mean error of 0.674 psi. The pump power shows a quadratic growth with the flow rate with a mean error of 0.49 W. Normally high electrolyte flow rate reduces the concentration overvoltage losses of VRB battery which benefits the stack voltage efficiency and performance, but high flow rate consumes more power for circulating the electrolyte. Thus, there is a tradeoff between the performance of the stack and the pumps' power consumption.

5. Analysis and discussion

Based on the proposed VRB model, the effects of the shunt current, terminal current density and electrolyte flow rate are analyzed in this section. The dynamic response of the proposed model is exhibited in the final part of this section.

5.1. The effect of shunt current

The variation of electrolyte tank SOC during the stack idling period is shown in Fig. 6(a). Here it has been assumed that the pumps continue to operate even if no charging or discharging is taking place. Due to the effect of shunt current, power loss exists even when the terminal current equals to zero when the pumps are operating. Under these conditions, the SOC of the electrolyte in the tanks decreases by 0.45% in 5 h. From Eq. (7), it is clear that the shunt current amplitude is directly influenced by the design of cell flow frame. The SOC fading or self-discharge caused by the shunt current is not obvious due to the appropriate design of cell flow frame. However, the impact of shunt current will become more severe if the series number of cells is increased. Moreover, in practical conditions, the operating time of storage equipment may last for several weeks and hence the SOC fading caused by the shunt current should not be ignored in the power system analysis. On the other hand, if the pumps are turned off during battery idling, the SOC of the electrolyte in the tanks will be unaffected, despite the fact that the stack electrolyte might become fully discharged as a result of the shunt current and ion diffusion processes across the membrane.

5.2. Effect of different current densities and electrolyte flow rates

To further demonstrate the feasibility of the proposed model in estimating VRB performance, the full cycle charge/discharge curves have been obtained as shown in Fig. 6(b). For avoid serious deviation, current density and electrolyte flow rate are chosen as 100–150 mA cm^{-2} and 3–5 L min^{-1} correspondingly. Both I and Q are within the known practical operating range. (The practical current density changes from 80 to 160 mA cm^{-2}, and the experimental electrolyte flow rate changes from 2 to 6 L min^{-1}) In all four curves, the initial SOC of tank is set to 0.15. The cells are charged to an SOC of 0.85 by a constant current and finally discharged to the initial state. From Fig. 6(b), it is clear that the charge/discharge curve is mainly affected by the current density and the flow rate.

As a known fact, higher current reduces charge/discharge time and increases the internal voltage loss. Hence the cycling time for 150 mA cm^{-2} is shorter than the cycling time for 100 mA cm^{-2}. And also, the voltage difference between charge and discharge for 150 mA cm^{-2} is higher than that for 100 mA cm^{-2}. On the other hand, as the concentration overpotential is reduced by increasing

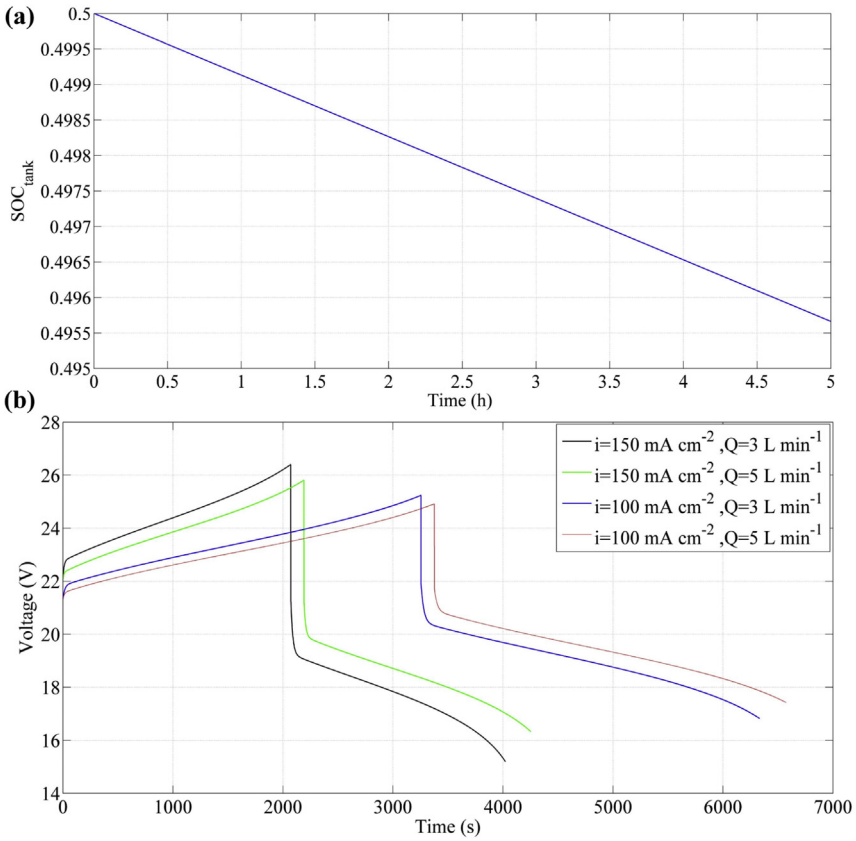

Fig. 6. Analysis of SOC self-discharging and charge/discharge cycles under different conditions, (a). SOC fading of tank electrolyte under stack idling condition with pump operation; (b). Terminal voltage during charge/discharge cycles at diverse current densities and flow rates.

the electrolyte flow rate, while the terminal voltage is decreased during charge and the opposite happens during discharge. In a practical battery management system, the stack terminal voltage is usually used as the threshold value for the charging/discharging process. A lower internal overpotential benefits the VRB system for deep charge/discharge cycles. The cycling time of the higher electrolyte flow rate is relatively long.

The proposed model can also assess the stack efficiencies during a series of charge/discharge cycles. The definition equations of energy efficiency and system efficiency are shown as follows [34],

$$\eta_{en} = \frac{\left| \int_0^{t_d} U_{dis}(t) i_{dis} dt \right|}{\int_0^{t_c} U_{cha}(t) i_{cha} dt} \tag{31}$$

$$\eta_{sys} = \frac{\left| \int_0^{t_d} \left(p_{dis} - p_{pump} \right) dt \right|}{\int_0^{t_c} \left(p_{cha} + p_{pump} \right) dt} \tag{32}$$

Fig. 7 (a) shows the effect of electrolyte flow rate on battery efficiency and Fig. 7(b) shows the effect of terminal current on battery efficiency. As represented in Fig. 7(a), the energy efficiency improves with the increase of electrolyte flow rate. Since high electrolyte flow rate leads to lower concentration overpotential and a higher SOC range during the charge/discharge processes, the energy efficiency of the VRB eventually increases. Nevertheless, the high flow rate leads to the high consumption of pump. Taking into account the fact that high flow rate increases the power consumption of the pumps, the system efficiency is a more appropriate term to evaluate the performance of VRB system. As shown in Fig. 7(a), the system efficiency increases quickly at the low flow rate stage due to the low pump consumption, while increasing gradually slow due to the high pump power consumption. An optimal flow rate must be attained which can balance the increase of energy efficiency as well as the power consumption of the pumps [35]. A more detail analysis has been demonstrated by Tang et al., considerable savings in pumping energy consumption can be achieved by using a variable flow-rate that is continuously adjusted to suit the operating current and SOC condition of the battery [20]. On the other hand, since a high terminal current aggravates the internal loss of battery, both energy efficiency and system efficiency decreases as the terminal current increased as shown in Fig. 7(b).

5.3. VRB dynamic response to the step current profiles

As this model is proposed for the application of power system analysis, it needs to predict the dynamic response under changing currents. From Fig. 8, it is clear that the terminal current densities change every 5 min and the initial tank SOC is set to 0.5. Based on the proposed VRB model, the variations of the stack terminal voltage and the tank SOC can be simulated at any time. For each current step, the unknown parameters of VRB model are estimated firstly based on the current density and the electrolyte flow rate. Combined with the effects of shunt current and ion diffusion, the SOC in the tank is obtained in the last plot of Fig. 8. By using the final electrical circuit model, the stack terminal voltage is estimated

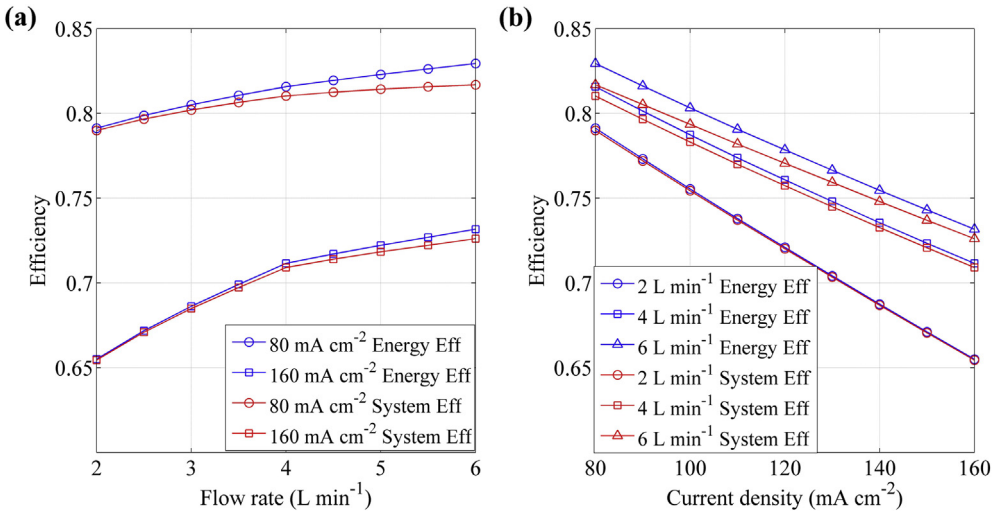

Fig. 7. Battery's efficiency under different flow rates and current density, (a). Under different flow rate; (b). Under different current density.

as represented in the middle plot of Fig. 8. It is worth noting that, the dynamic response caused by the R_1C_1 chain is also predictable by using this model. When the power electronics for the VRB stack are designed, the dynamic characteristics of VRB is important to be obtained for the control loop design. By known the R1C1 chain, the frequency-domain's characteristic of VRB can be simply estimated.

6. Conclusion

In this paper, the modeling method of VRB system has been investigated. Based on the practical VRB system proposed by Kim [22], a complete equivalent circuit model has been proposed for power system analysis. The model consisting of an open-circuit voltage (OCV) source, two parallel current sources, a 1st order resistor-capacitor network and a hydraulic model. The OCV source is described by the modified Nernst potential based on state-of-charge (SOC). Two parallel current sources represent the effects of shunt current and ion diffusion. The 1st order resistor-capacitor network depicts both dynamic and stationary characteristics of the VRB stack. The hydraulic model gives an empirical method to analyze pump power. Based on the time scale of battery operation, the dynamic and stationary characteristics of VRB are identified by using least square method. Moreover, by considering the effects of shunt current and hydraulic losses, the proposed model can also predict the SOC fading during idling as well as the pump power consumption. All of these parameters are crucial for battery management and converter design. Validated with experimental data, the model demonstrates a good degree of accuracy. The mean-error of stack terminal voltage and pump consumption equal to 0.09 V and 0.49 W correspondingly.

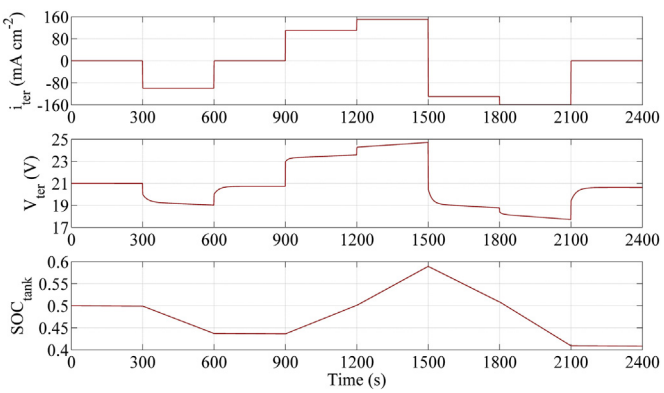

Fig. 8. Battery response under current steps at the flow rate equals of 4 L min^{-1}.

Based on the proposed model, several sensitivity studies have been done to further understand the VRB system. It is found that the battery performance is significantly influenced by the electrolyte flow rate. As the pump power consumption exhibits a quadratic growth with the flow rate, the system efficiency does not improve monotonically with the increase of electrolyte flow rate. These factors necessitate the requirement for an optimal flow rate strategy to maximize the system efficiency, which is similar with the conclusion of Tang [20].

Furthermore, the proposed model can predict the dynamic response of VRB under changing terminal currents where both SOC and the stack terminal voltage can be obtained.

However, the current model lacks of the thermal model as well as the detailed ion diffusion model. The primary goal of this paper is to capture the major features of VRB system and represent in a simple form for the application in electrical system. The electrical interface design and the battery management system based on this VRB model would be analyzed in future.

References

[1] Z.G. Yang, J.L. Zhang, M.C.W. Kintner-Meyer, X.C. Lu, D.W. Choi, J.P. Lemmon, J. Liu, Chem. Rev. 111 (2011) 3577–3613.
[2] M.H. Chakrabarti, S.A. Hajimolana, F.S. Mjalli, M. Saleem, I. Mustafa, Arab. J. Sci. Eng. 38 (2013) 723–739.
[3] E. Sum, M. Rychcik, M. Skyllas-Kazacos, J. Power Sources 16 (1985) 85–95.
[4] M. Skyllas-Kazacos, M. Rychcik, R.G. Robins, A.G. Fane, M.A. Green, J. Electrochem. Soc. 133 (1986) 1057–1058.
[5] M. Skyllas-Kazacos, M.H. Chakrabarti, S.A. Hajimolana, F.S. Mjalli, M. Saleem, J. Electrochem. Soc. 158 (2011) R55–R79.
[6] W. Wang, Q.T. Luo, B. Li, X.L. Wei, L.Y. Li, Z.G. Yang, Adv. Funct. Mater. 23 (2013) 970–986.
[7] B. Schwenzer, J. Zhang, S. Kim, L. Li, J. Liu, Z. Yang, ChemSusChem 4 (2011) 1388–1406.
[8] H. Al-Fetlawi, A.A. Shah, F.C. Walsh, Electrochimica Acta 55 (2009) 78–89.
[9] M.H. Li, T. Funaki, T. Hikihara, in: Power Conversion Conference - Nagoya, 2007. PCC '07, 2007, pp. 221–225.
[10] A.A. Shah, M.J. Watt-Smith, F.C. Walsh, Electrochimica Acta 53 (2008) 8087–8100.
[11] I.A. Chidambaram, B. Paramasivam, J. Power Sources 219 (2012) 292–304.
[12] A. Shibata, K. Sato, Power Eng. J. 13 (1999) 130–135.
[13] J. Chahwan, C. Abbey, G. Joos, in: Electrical Power Conference 2007, EPC 2007. IEEE Canada, 2007, pp. 387–392.
[14] R.L. Fares, J.P. Meyers, M.E. Webber, Appl. Energy 113 (2014) 189–198.
[15] J.G. Zhu, Z.C. Sun, X.Z. Wei, H.F. Dai, J. Power Sources 274 (2015) 990–1004.

[16] M.R. Mohamed, H. Ahmad, M.N. Abu Seman, S. Razali, M.S. Najib, J. Power Sources 239 (2013) 284–293.
[17] A. Tang, J. McCann, J. Bao, M. Skyllas-Kazacos, J. Power Sources 242 (2013) 349–356.
[18] F.T. Wandschneider, S. Rohm, P. Fischer, K. Pinkwart, J. Tubke, H. Nirschl, J. Power Sources 261 (2014) 64–74.
[19] B.Y. Xiong, J.Y. Zhao, K.J. Tseng, M. Skyllas-Kazacos, T.M. Lim, Y. Zhang, J. Power Sources 242 (2013) 314–324.
[20] A. Tang, J. Bao, M. Skyllas-Kazacos, J. Power Sources 248 (2014) 154–162.
[21] C. Blanc, A. Rufer, in: Sustainable Energy Technologies, ICSET 2008. IEEE International Conference on, 2008, 2008, pp. 696–701.
[22] S. Kim, E. Thomsen, G. Xia, Z. Nie, J. Bao, K. Recknagle, W. Wang, V. Viswanathan, Q. Luo, X. Wei, A. Crawford, G. Coffey, G. Maupin, V. Sprenkle, J. Power Sources 237 (2013) 300–309.
[23] M. Skyllas-Kazacos, M. Kazacos, J. Power Sources 196 (2011) 8822–8827.
[24] B. Xiong, J. Zhao, Z. Wei, M. Skyllas-Kazacos, J. Power Sources 262 (2014) 50–61.
[25] S. Corcuera, M. Skyllas-Kazacos, Eur. Chem. Bull. 1 (2012) 511–519.
[26] J.A. Schaeffer, L.D. Chen, J.P. Seaba, J. Power Sources 182 (2008) 599–602.
[27] R.E. White, C.W. Walton, H.S. Burney, R.N. Beaver, J. Electrochem Soc. 133 (1986) 485–492.
[28] S. Kim, J. Yan, B. Schwenzer, J. Zhang, L. Li, J. Liu, Z. Yang, M.A. Hickner, Electrochem. Commun. 12 (2010) 1650–1653.
[29] R. Badrinarayanan, J.Y. Zhao, K.J. Tseng, M. Skyllas-Kazacos, J. Power Sources 270 (2014) 576–586.
[30] X.F. Li, H.M. Zhang, Z.S. Mai, H.Z. Zhang, I. Vankelecom, Energ. Environ. Sci. 4 (2011) 1147–1160.
[31] A. Tang, J. Bao, M. Skyllas-Kazacos, J. Power Sources 196 (2011) 10737–10747.
[32] L.J. Ontiveros, P.E. Mercado, Int. J. Hydrogen Energy 39 (2014) 8720–8727.
[33] F. Baccino, M. Marinelli, P. Norgard, F. Silvestro, J. Power Sources 254 (2014) 277–286.
[34] L. Li, S. Kim, W. Wang, M. Vijayakumar, Z. Nie, B. Chen, J. Zhang, G. Xia, J. Hu, G. Graff, J. Liu, Z. Yang, Adv. Energy Mater. 1 (2011) 394–400.
[35] X.K. Ma, H.M. Zhang, C.X. Sun, Y. Zou, T. Zhang, J. Power Sources 203 (2012) 153–158.